Eur Radiol (2011) 21:604–615
DOI 10.1007/s00330-010-1965-6

ULTRASOUND

Assessment of tissue perfusion by contrast-enhanced ultrasound

Emilio Quaia

Received: 31 May 2010 / Revised: 13 August 2010 / Accepted: 17 August 2010 / Published online: 7 October 2010

Abstract Contrast-enhanced ultrasound (CEUS) with microbubble contrast agents is a new imaging technique for quantifying tissue perfusion. CEUS presents several advantages over other imaging techniques in assessing tissue perfusion, including the use of microbubbles as blood-pool agents, portability, availability and absence of exposure to radiation or nuclear tracers. Dedicated software packages are necessary to quantify the echo-signal intensity and allow the calculation of the degree of tissue contrast enhancement based on the accurate distinction between microbubble backscatter signals and native tissue background. The measurement of organ transit time after microbubble injection and the analysis of tissue reperfusion kinetics represent the two fundamental methods for the assessment of tissue perfusion by CEUS. Transit time measurement has been shown to be feasible and has started to become accepted as a clinical tool, especially in the liver. The loudness of audio signals from spectral Doppler analysis is used to generate time-intensity curves to follow the wash-in and wash-out of the microbubble bolus. Tissue perfusion may be quantified also by analysing the replenishment kinetics of the volume of microbubbles after their destruction in the imaged slice. This allows to obtain semiquantitative parameters related to local tissue perfusion, especially in the heart, brain, and kidneys.

Keywords Ultrasound · Microbubble · Contrast agents · Contrast-enhanced ultrasound · Tissue perfusion

E. Quaia (✉)
Department of Radiology, Cattinara Hospital,
University of Trieste (Italy),
Strada di Fiume 447,
Trieste 34149, Italy
e-mail: quaia@units.it

Introduction

The ability to accurately quantify tissue perfusion, blood flow equalised for the volume or weight of the perfused tissue ($cm^3/s/cm^3$ or grams), is essential for the assessment of the physiological functionality and viability of a tissue. Different parameters are related to tissue perfusion including: blood velocity (cm/s), the speed of red blood cells in the region analysed; blood flow (cm^3/s), the volume of blood passing in a section of tissue per unit of time; the fractional vascular volume (cm^3), the proportion of tissue volume occupied by blood.

Laser Doppler [1], single photon computed tomography (SPECT) [2], multidetector computed tomography (CT) [3], magnetic resonance (MR) imaging [4] and positron emission tomography (PET) [5] all quantify tissue perfusion accurately but they are expensive and present some inherent limitations such as limited availability and patient exposure to radiation or nuclear tracers. Colour and power Doppler are limited by the low sensitivity to low-velocity flow in smaller vessels (<2 mm in diameter). Contrast-enhanced ultrasound (CEUS) with microbubble contrast agents [6–8] has recently been proposed as a new imaging technique for quantifying tissue perfusion [9, 10]. CEUS presents several advantages including low cost, portability, availability, lack of restrictions in performing serial examinations at short intervals, and absence of exposure to radiation or nuclear tracers.

Microbubble contrast agents

Microbubble contrast agents for ultrasound (US) (Table 1) have a diameter of 2 to 6 μm (Fig. 1). The microbubble shell may be stiff (e.g. denaturated albumin) or flexible

(phospholipids) and has a thickness of 10 to 200 nm. New-generation microbubbles are filled with a high-molecular-weight gas (e.g. perfluorocarbon or sulphur hexafluoride) with low solubility in the bloodstream. Microbubbles have a purely intravascular distribution even though some agents present a post-vascular hepato- and/or spleno-specific phase beginning 5 min after i.v. injection and lasting from 15 min up to 1 h after injection [11, 12]. The microbubble gas content is exhaled via the lungs 10 to 15 min after injection while the components of the shell are metabolised by the liver or filtered by the kidney. Adverse reactions in humans are rare, usually transient, and of mild intensity [13, 14]. Hypotensive reactions have been observed after microbubble injection, and some deaths have been reported in cardiac patients [15–18].

At resonant frequency (f_o) the microbubble radial oscillation becomes efficient and exaggerated; the scattering cross section of a microbubble is no longer simply dependent on microbubble size, and can reach peak values a thousand times higher than values at off-resonance. The insonation power is usually expressed by the mechanical index (MI) defined as $p-/\sqrt{fc}$ where $p-$ is the largest peak negative pressure and fc is the centre frequency of the pulse. When acoustic pressures at or near the resonant frequency are sufficiently high, non-linear microbubble oscillation develops producing harmonic frequencies. These frequencies allow us to distinguish microbubble signal from tissue clutter by using specialised contrast-specific US techniques. Pulse Inversion is the best-known phase-modulation technique. Vascular Recognition Imaging combines Doppler information with phase analysis and involves the transmission of four, alternately inverted, pulses along each imaging line. Cadence Contrast Pulse Sequencing works by interrogating each imaging line a number of times with pulses with various amplitudes and phases. Both harmonic and non-linear fundamental signals from microbubbles are represented on a grey-scale or colour map suppressing the linear fundamental echoes from native tissues.

Table 1 Microbubble contrast agents classified according to the filling gas

Perfluorocarbon	Sulphur hexafluoride
- Definity (Lantheus Medical Imaging) - Sonazoid (GE Healthcare) - Optison (GE Healthcare)[a]	- SonoVue (Bracco)

The list include the presently available microbubble contrast agents

Imavist (Imagent; Alliance), Quantison (Quadrant), and Echogen (Sonus Pharmaceuticals) did not achieve the clinical use. Echovist and Levovist (Bayer-Schering) and Albunex (Mallinckrodt) are not presently employed. Cardiosphere (Point Biomedical) is no longer developed. One other agent, Zhifuxian, is being developed by Chinese hospitals and is nearing clinical use

All available agents present a phospholipid shell. SonoVue is currently approved and marketed within European countries. Definity is approved in USA for cardiology and in Canada for liver imaging, while Sonazoid (GE Healtcare) is licensed in Japan for liver imaging

In perfluorocarbon-filled agents the filling gas is perfluorobutane (e.g. Optison and Sonazoid), octafluoropropane (e.g. Definity), or perfluorohexane (e.g. Imagent)

[a] Albumin shell; recently re-released to the market

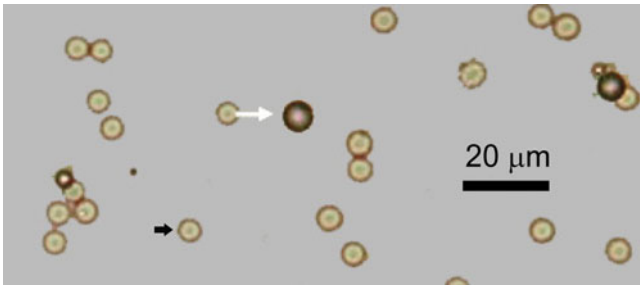

Fig. 1 Two-dimensional microscopic photo of SonoVue (*white arrows*) microbubbles (20× magnification; optical microscope) compared with red blood cells (*black arrows*)

Transit time measurements

Tracking the transit of a bolus of microbubbles enables measurements of the physiology of organs. The loudness of audio signals from spectral Doppler analysis can be used to generate time-intensity curves to follow the wash-in and wash-out of the microbubble bolus. In the kidney, where the adjacent position of the artery and the vein enables spectral Doppler measurement, the signal rises as the microbubble bolus arrives first in the artery and then in the vein and the directionality of spectral Doppler allows these two signals to be separated. In the normal kidney the arterial venous transit is less than 4 s, while it is increased in acute renal allograft rejection [19]. The true mean transit time can be calculated by plotting the arterial and venous time intensity curves, applying a gamma-variate fit to select the first pass of the contrast agent, discarding signals from recirculating contrast, and then calculating the difference between the centroids of the two curves. In the breast, many studies showed that both transit time [20] and arrival time [21, 22] in cancers is shorter than in benign masses.

In the liver, the delay between injection or arrival in the hepatic artery and the first appearance of contrast agent in a hepatic vein can be measured. To this end, a hepatic vein is targeted and kept in the field of view before the microbubble injection is given with the patient breathing quietly (Fig. 2). In normal subjects, the arrival time in the hepatic vein after peripheral i.v. injection usually occurs after 30 s (Fig. 3a) (the lower limit of normal was found to be 25 s) [23, 24]. In cirrhosis, an early arrival time of the contrast bolus (<24 s) and a left shift of the time-intensity curve are

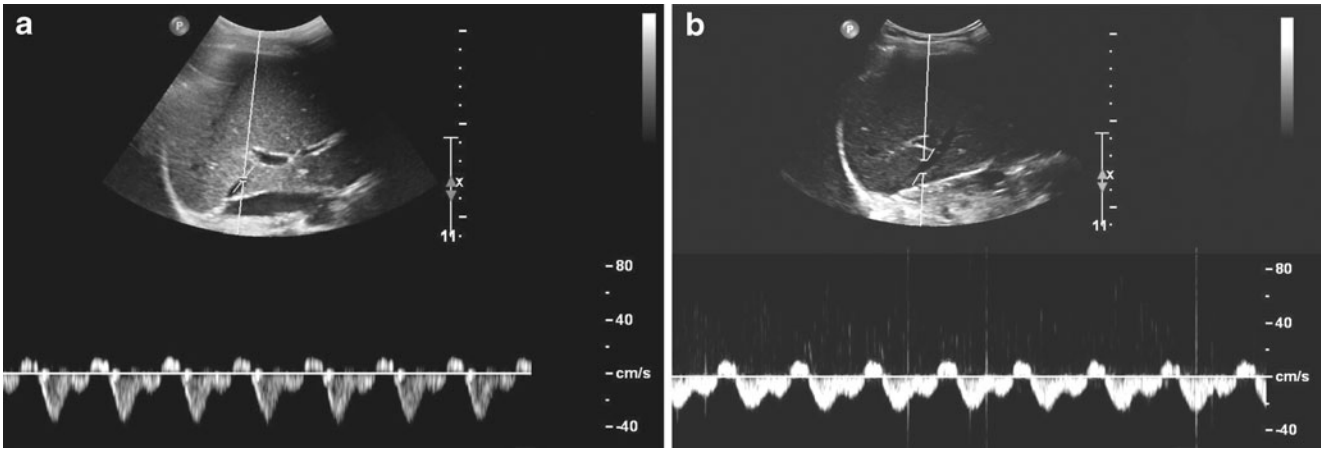

Fig. 2 Spectral Doppler for hepatic vein transit time measurement. The spectral Doppler sample volume is placed on a hepatic vein before injection of the contrast agent, in this case sulphur hexafluoride-filled microbubbles (**a**), and the time when the signal increases (**b**) is noted. The audio output is fed into a laptop computer and the moment the signal increases consistently above 10% over baseline is taken as the arrival time

seen because of a hepatic arterial supply and the presence of intrahepatic shunts (Fig. 3b). This test was also shown to be accurate in assessing the severity of diffuse liver disease [25], and in separating between mild and moderate/severe chronic hepatitis [26]. Hepatic vein transit time was shown to be significantly shorter with sulphur hexafluoride-filled than with air-filled microbubbles, even though there was more effective differentiation between moderate or severe hepatic fibrosis or cirrhosis from normal volunteers with Levovist than with SonoVue [27]. As a further field of application, arrival time has been studied in patients with metastatic disease of the liver, and a left shift of the time-intensity curve and a typical cut-off value of <24 s were observed [23, 28].

Objective analysis of echo-signal intensity

Determination of the degree of tissue contrast enhancement relies on the accurate distinction between microbubble

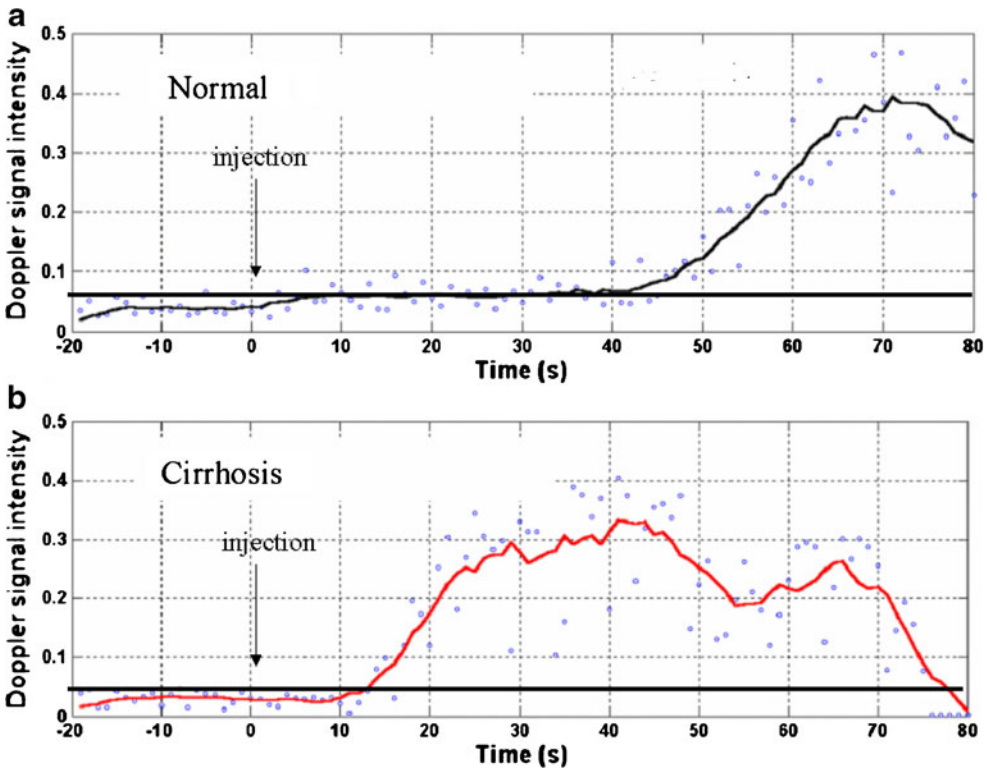

Fig. 3 Time-intensity curve. These curves have been calculated from the loudness of Doppler signals after a bolus injection of a contrast agent with the sample volume placed on a hepatic vein. The raw data, shown as multiple dots, has a phasic variation caused by echo-signal variability while the interpolating line is the result of applying a nine-point smoothing algorithm. Many temporal and quantitative features can be calculated from such curves. **a** Normal transit time profile in a patient with normal liver; **b** Early arrival of microbubbles with reduced transit time in a patient with liver cirrhosis (reproduced with permission from Gut [26])

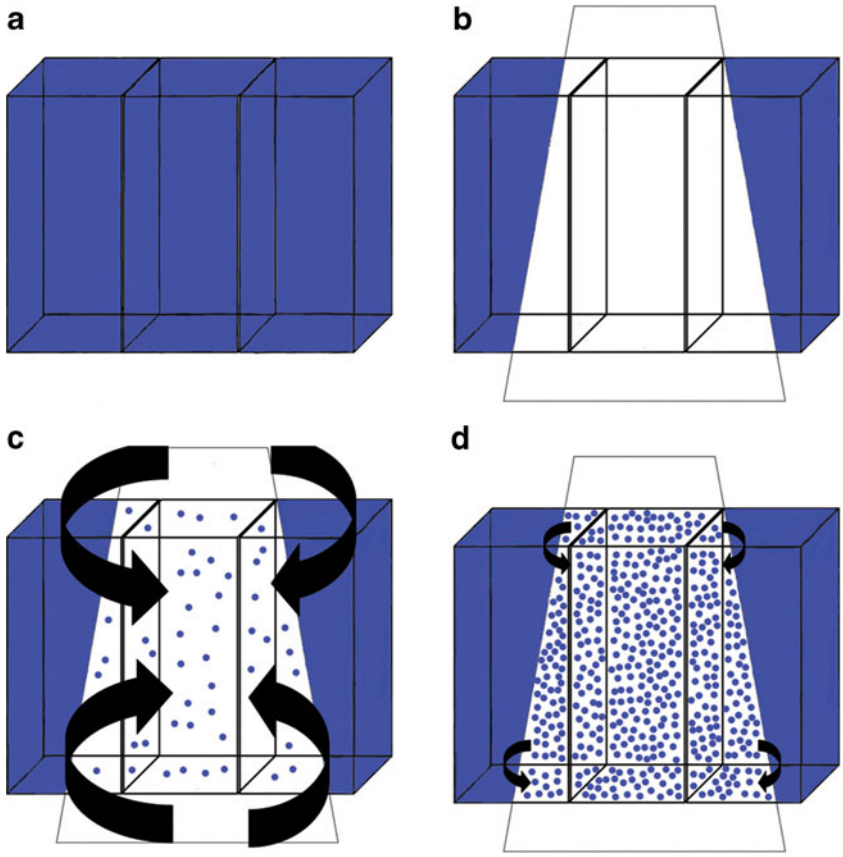

Fig. 4 Progressive refilling of the imaged volume after microbubble destruction following high-transmit-power insonation. **a** Microbubbles are filling three adjacent tissue volumes after the achievement of a steady-state concentration in the peripheral circulation; **b** high-transmit-power insonation destroys the microbubbles in the insonation field and creates a microbubble void in the imaged volume; **c**, **d** the microbubble void is progressively re-filled by microbubbles coming from the adjacent regions and not in the insonation field

backscatter signals and stationary tissue background. The fundamental assumption is the linear relation between video-intensity and microbubble concentration up to the achievement of a plateau phase [29]. After achievement of the plateau phase microbubble concentration increases while videointensity remains constant, and at even higher concentrations, the video intensity actually decreases because of attenuation of the US beam by the microbubbles themselves. Quantitative analysis of tissue perfusion using CEUS is still limited by acoustic shadowing owing to the inadequate compensation for microbubble attenuation, and tissue attenuation correction algorithms or mathematical

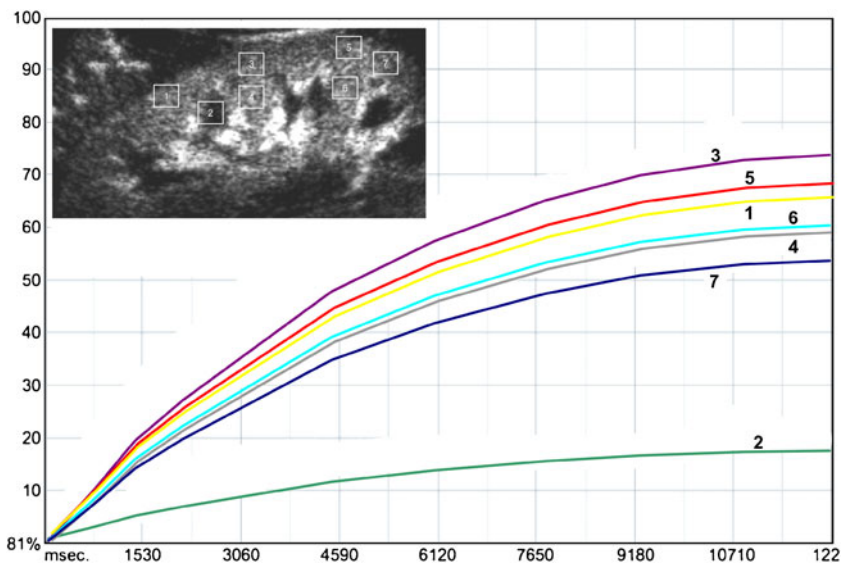

Fig. 5 Quantitation of renal perfusion by contrast-enhanced US, after sulphur hexafluoridefilled microbubble injection at low-acoustic-power insonation. The upper figure represents the position of the multiple square regions of interest (ROIs) on the renal cortex excluding the renal medulla (ROI 1 and ROIs 3 – 7), except for one ROI including the renal medulla (ROI 2).The difference in blood kinetics between renal cortex and medulla is visualized by the different curve profile since renal medulla (curve 2) presents a much lower perfusion (190 ml/min/100 g) compared with renal cortex (400 ml/min/100 g) represented by a lower slope of the first ascending tract and a lower value of the plateau phase

models estimating microbubble attenuation have been proposed [30, 31].

Backscatter signals from microbubbles are processed into pixels of brightness for video presentation in the US system in order to express echo-power values that reflect instantaneous in situ concentration of microbubble contrast agents. The translation of echo amplitude values to a scale of display brightness or color appropriate to human visual perception is performed through a series of steps. Logarithmic compression is employed for displaying signals with a large dynamic range on US monitors that have smaller dynamic ranges. Beside logarithmic compression, other methods are employed to provide pleasing images at visual perception including the use of different post-processing curves or color maps and signal filtering for edge enhancement. Time-intensity curves may be calculated by positioning a manually defined or automatically copied region of interest (ROI) over a parenchymal region and by correlating the measured video intensity (VI: 0–255 grey-scale levels) with time in seconds [30, 31]. Based on the mathematics of logarithms the mean video intensity in an ROI is:

$$\text{mean VI} = \frac{1}{N} \times \sum_{j=1}^{N} 10\log_{10}\left(\frac{I_j}{I_{ref}}\right)$$

where N indicates the pixel number within the ROI, I_j is the acoustic intensity and I_{ref} is an intensity reference level determined through equipment gain [32].

The direct visual assessment of the degree of log-compressed video-intensity is the least accurate method because the background tissue signal varies widely within the US sector, because of heterogeneities of acoustic power and differences in the attenuation and absorption of US energy by tissue. A practical approach consists of collecting imaging-converted video data, log-compressed and palletised as grey-scale or colour-coded 8-bit data, in the form of DICOM files. In this case, however, proper linearisation needs to be applied before curve-fitting and analysis, in order to reverse the effects of log-compression and possibly

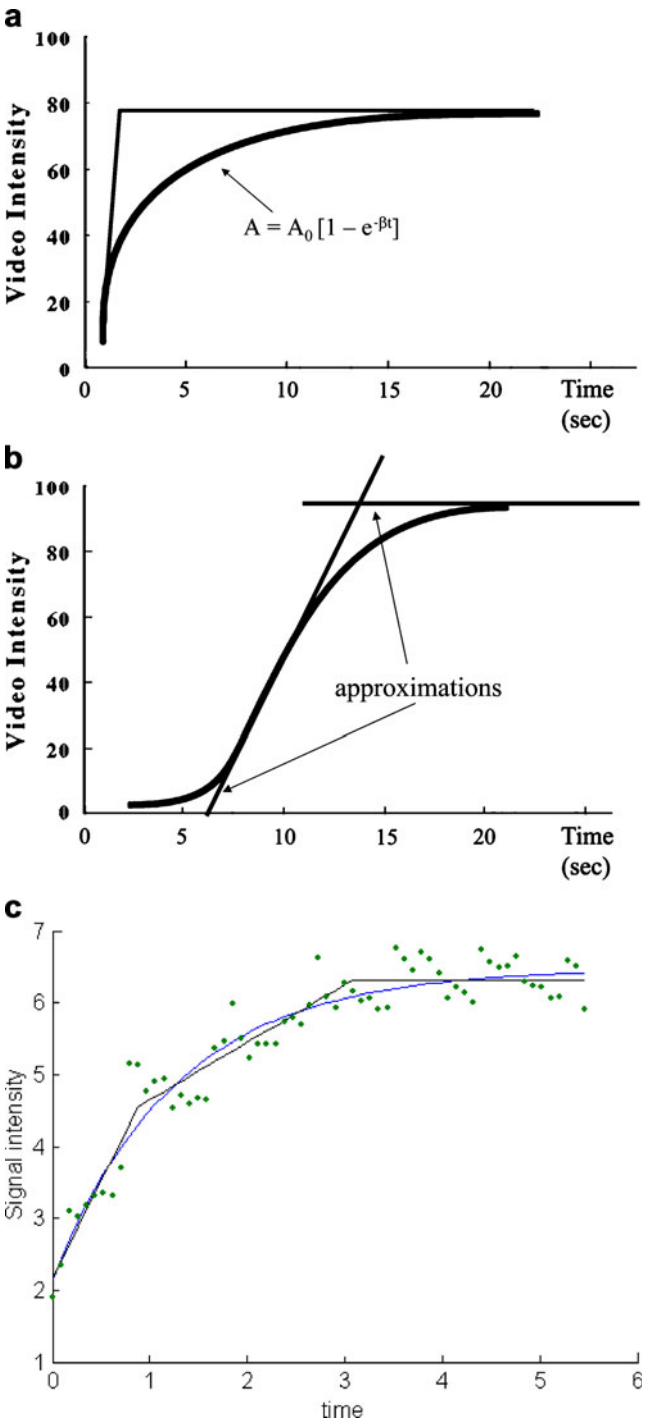

Fig. 6 Different functions that have been proposed to approximate the refilling kinetics in tissues. **a** Negative exponential curve; β=slope of the first ascending tract (~ blood flow velocity), A=maximum amplitude of the re-filling curve (~fractional blood volume). The distortion from the linear model is due to microbubble diffusion within the vessels during the arrival time. **b** Sigmoid curve [48] expressed by the equation $C_n(t) = \frac{C_0}{(1+\tau\lambda)^n} \times \left[1 - \left(1 + \sum_{i=1}^{n-1} \frac{\beta^i t^i}{i!}\right) e^{-\beta t}\right]$, where $C_n(t)$ is the refilling evolution of the microbubble concentration in the subvolume n, C_0 is the concentration of microbubbles in blood vessels that enter the ROI (number of microbubbles per litre) which is assumed to be constant with time, t is time, λ represents the fraction of microbubbles destroyed by the US beam per second which is assumed to be constant, $1/\tau = F/V_b$ where F is the rate of the inflow (equal to the rate of outflow) and Vb is the volume of flow in the ROI, and β is equal to: $(1+\tau\lambda)/\tau$). The approximation lines indicate the curve shape without considering the percentage of microbubbles destroyed by low-transmit-power insonation. The distortion from the linear model is due to the percentage of microbubbles destroyed by low transmit power insonation. **c** Comparison between the echo-signal (linear scale) data set approximation obtained by a negative exponential function (mean square error, 0.2) and by piecewise linear function with 2 linear tracts (mean square error, 0.15) both obtained in a human kidney

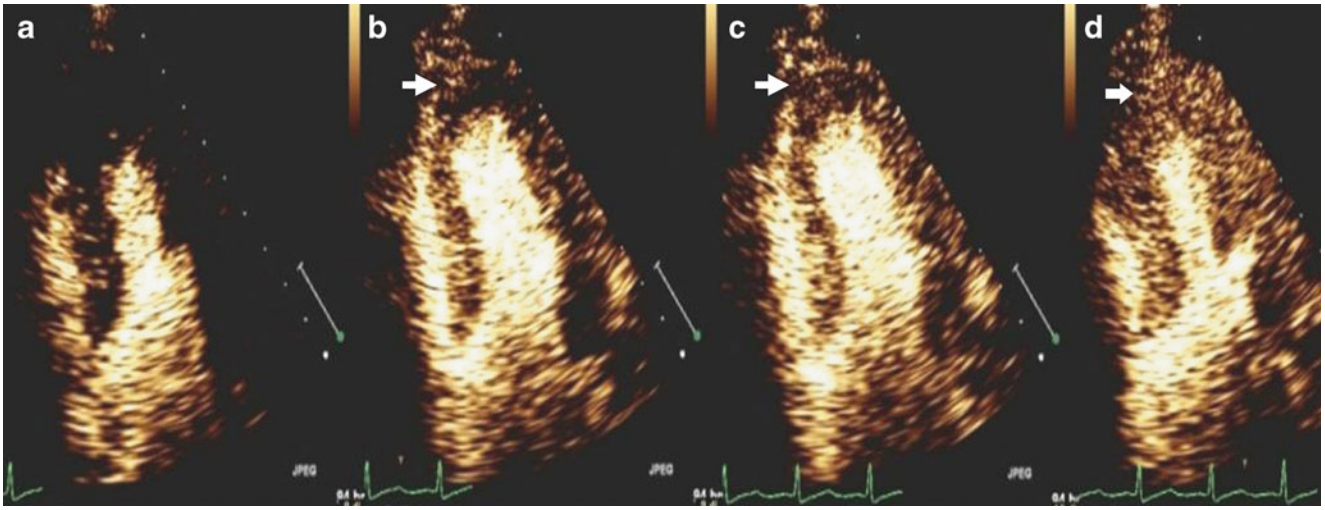

Fig. 7 Apical perfusion defect (*arrows*) visualised on contrast myocardial echocardiography. In the apical myocardium vascularised by a stenotic coronary artery the rate of refilling is slower (**a**–**d**) in comparison to the other myocardial regions (courtesy from doctor Gaibazzi, Parma)

non-linear palette rendering [33]. The quantitation of echo-signal intensity after anti-logarithmic transformation is the most accurate method, and eliminates the influence of logarithmic compression, colour maps, postprocessing curves, and techniques for edge enhancement on the input signal mapping for video presentation. Software packages access the raw data before application of non-linear modifications and allow image alignment, signal averaging and background subtraction.

A parametric image is an image where each pixel/voxel value represents the value of given parameters (e.g. blood flow or velocity or tissue perfusion) derived from multiple images at that location. Parametric images may be obtained after background subtraction in a pixel-by-pixel evaluation from the analysis of harmonic grey-scale imaging data through the use of dedicated software packages for the automated colour-coded depiction of the different kinetic parameters [34, 35].

Reperfusion methods

The achievement of a steady-state microbubble concentration in the peripheral circulation is preferable in tissue perfusion studies [36]. When microbubbles are administered as a constant infusion, the steady state is achieved after 2–3 min. This is obtained by dedicated microbubble injectors usually equipped with a rotating syringe to avoid microbubble sedimentation. At steady state the inflow and outflow of microbubbles in any microcirculatory unit is constant, proportional to the fractional blood volume of that unit, and dependent only on the flow rate of microbubbles.

Local tissue perfusion may be calculated by analysing the replenishment kinetics of the volume of microbubbles after their destruction by initial high-transmit-power insonation [37, 38]. After microbubble destruction the system is switched to a low transmit power so that the refill rate of microbubbles returning to the imaged volume can be monitored (Fig. 4). One of the main limitations of the technique is that perfusion data are acquired from a single tissue plane, a situation unlikely to accurately reflect global perfusion of the tissue or organ under consideration. The 3-D volumetric haemodynamics of the reperfusion are complex and have not yet been fully modelled. The opposite approach, known as diminution kinetics [39, 40], can also be implemented, i.e. by observing the rate of decay of microbubbles exposed to a high intensity beam, but this cannot be performed in real time.

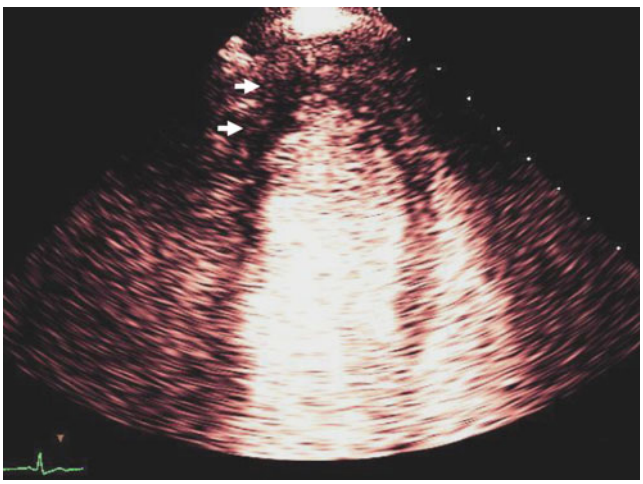

Fig. 8 Contrast myocardial echocardiography after sulphur hexafluoride-filled microbubble injection. Reversible apical and infero-lateral myocardial perfusion defect (*arrows*) visualised under pharmacological stress (courtesy from Bracco Imaging)

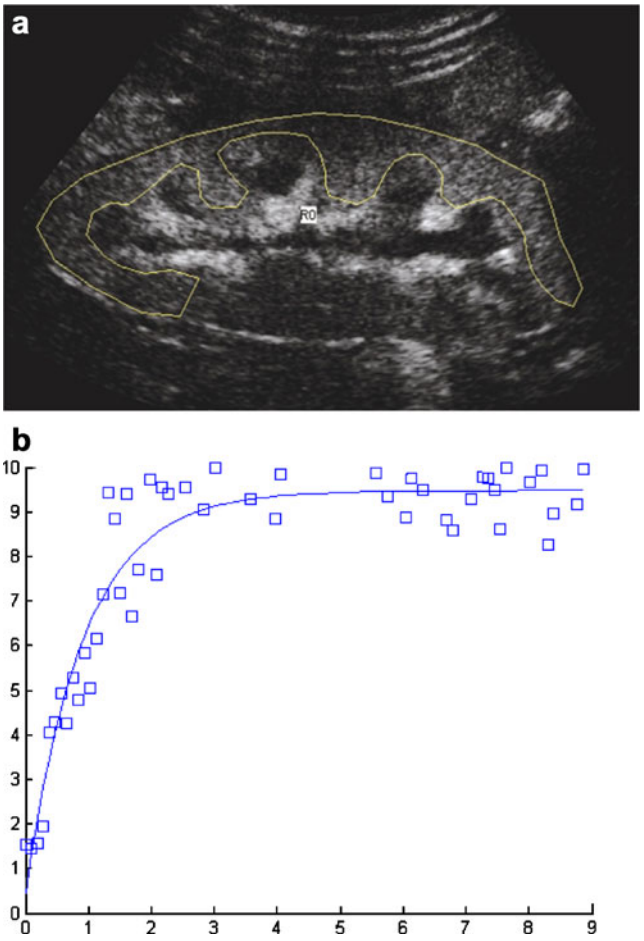

Fig. 9 Normal refilling curve measured in a kidney of a 45-year-old volunteer. **a** The echo-signal intensity is quantified by a manually-defined ROI positioned over a region of renal parenchyma excluding renal medulla by proprietary software (HDI Lab, version 1.90a and Qlab, version 3.0; Advanced Technology Laboratories–Philips). **b** Linear echo-signal intensity data were plotted vs time and fitted according to a negative exponential function by the software MATLAB 7.0.1 (The MathWorks, Natick, MA, USA)

The analysis of the refilling process (Fig. 5) provides semiquantitative data related to tissue perfusion values [36, 41, 42]. These include time to peak intensity, the initial slope of the refill (β~blood flow velocity), the maximum amplitude of the re-filling curve (A~fractional blood volume), the area under the curve (~blood volume) and the mean transit time. According to the central volume theorem tissue perfusion may be calculated as the ratio of the fractional vascular volume to the mean transit time [43]. The product of A (cm^3/g of tissue)×β (s^{-1}), corresponding to the area under the curve, is correlated with perfusion. Unfortunately, this cannot be converted to true perfusion as the volume of the perfused tissue is not known because the beam thickness and shape are complex and dependent on machine settings (e.g. the focus position) and patient variables (e.g. attenuation).

Mathematical models for perfusion quantification

Different mathematical models have been proposed to fit the refilling kinetics. In the first model [36, 44, 45], the exponential behaviour is a consequence of microbubble diffusion and the refill curve has a rising exponential form described by the equation:

$$\text{Signal intensity} = A(1 - e^{-\beta t}).$$

Unfortunately, the exponential function (Fig. 6a) does not take into account the fluid dynamics including the different blood velocity during systole and diastole and the different velocity profile of arteries and veins, and it fails to

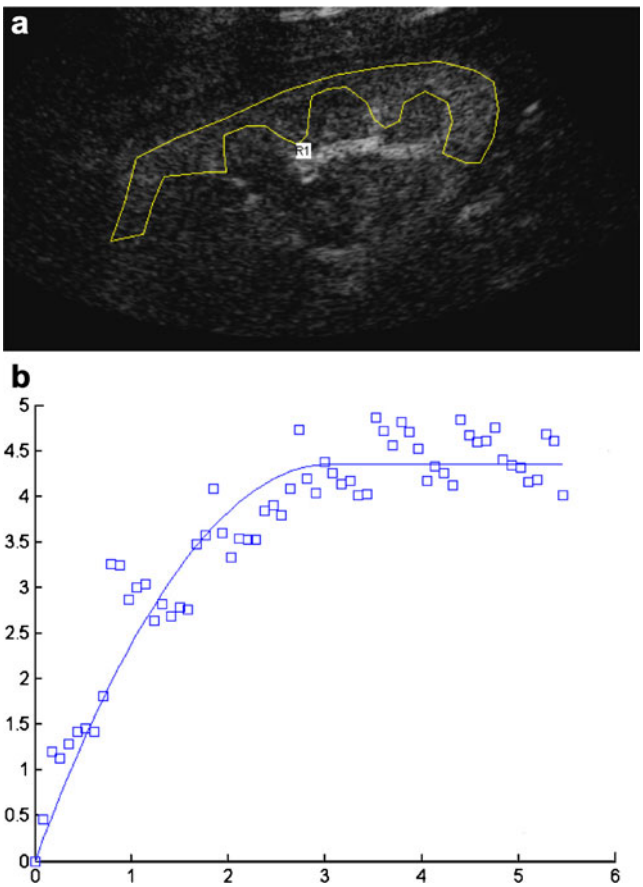

Fig. 10 Reduced renal parenchymal perfusion due to renal artery stenosis in patients without any pharmacological treatment. **a** The echo-signal intensity is quantified in a manually-defined ROI positioned over a region of renal parenchyma excluding the renal medulla by proprietary software (HDI Lab, version 1.90a and Qlab, version 3.0; Advanced Technology Laboratories–Philips). **b** Linear echo-signal intensity data were plotted vs time and fitted according to a negative exponential function by the software MATLAB 7.0.1 (The MathWorks, Natick, MA, USA). In comparison to the case in Fig. 9a lower slope of the first ascending tract of the curve (related to the blood flow velocity) and a lower plateau phase (related to the fractional vascular volume) is observed

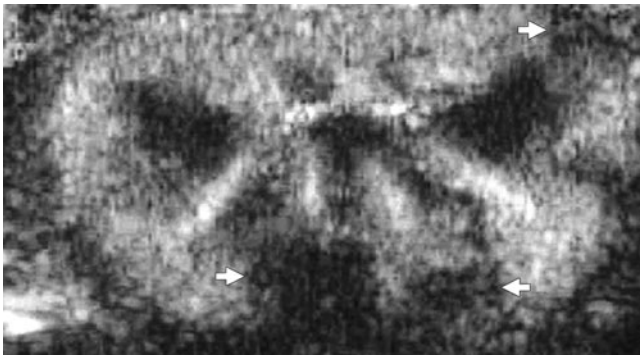

Fig. 11 Renal parenchyma perfusion defect after microbubble injection in a New Zealand white rabbit. In all animals the abdominal aorta and both kidneys were surgically exposed after midline laparotomy. The blood flow was stopped by manual compression of the sub-renal abdominal aorta for approximately 5 s, while 2 ml of polyvinyl alcohol embolising particles (150–250 μm in diameter) were injected directly into the supra-renal abdominal aorta, below the level of the superior mesenteric artery and coeliac trunk, through a 22-gauge needle. This procedure caused random occlusion of one or more renal segmental arteries, with the production of focal ischaemic renal perfusion defects. The multiple perfusion defects (*arrows*) are clearly visible after microbubble injection

predict the experimental results if the percentage of microbubble destruction in the vessels feeding the ROI is not null. Further limitations of this model include the assumption of a constant concentration of microbubbles entering the ROI immediately after the destruction pulse and the neglect of the different directions of the vessels inside the examined ROI.

Potdevin et al. [37, 38] developed a dual model with a cross-plane and an in-plane vascularity for both the renal medullary and cortical regions, in which the whole refilling process is a weighted average of all possible elemental refill curves. Krix et al. [46] proposed a multivessel model that neglects diffusion, the microbubble movement from an area of high concentration to an area of lower concentration, and does not present exponential features, but assumes and takes into account a particular geometry of the vessels in the ROI. In all these mathematical models the time-intensity curves frequently present a wide data dispersion during both the ascending and the second plateau phase of the curve [47]. Lucidarme et al. [48] proposed a model described by a sigmoid function (Fig. 6b) which is based on the assumption that microbubble destruction actually occurs in the feeding vessels that reach the ROI. Another model [49] states that the refilling kinetics depends on the distribution of vessel transit times and flows in the kidney, resulting in a piecewise linear function where the transit times are the times that separate the linear tracts, and the slopes are directly related to the flows (Fig. 6c).

Clinical applications of organ perfusion

In humans, CEUS has been applied to quantify brain perfusion in acute cerebral stroke [50–54]. In cardiac imaging, CEUS has an established role in left ventricle opacification and endocardial border definition to assess myocardial function and ejection fraction [55–57]. The quantification of myocardial perfusion through reperfusion kinetics [57, 58] is accurate in the detection of coronary artery stenosis [59], and provides similar results to SPECT and stress echocardiography [60]. In normal conditions during pharmacological stress, the myocardium is fully replenished by microbubbles 1 to 1.5 s after the end of a high-transmit-power pulse train [58], while in regions subserved by stenotic coronary arteries the rate of filling is slower depending upon the severity of stenosis (Fig. 7). The filling abnormalities are frequently seen to be more

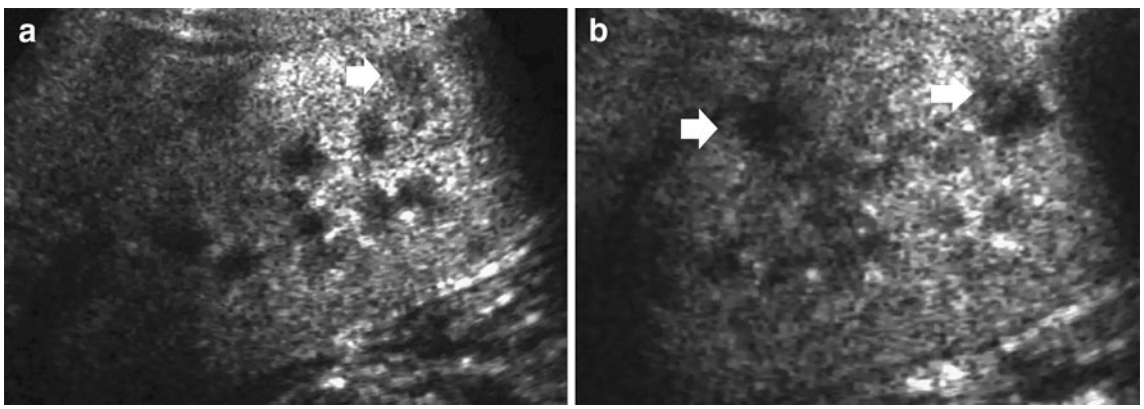

Fig. 12 Renal artery embolisation in an 82-year-old male patient presenting at the emergency unit with acute right-sided flank pain. Contrast-enhanced ultrasound after sulphur hexafluoride-filled microbubble injection. Multiple bilateral renal parenchymal perfusion defects (*arrows*), involving mainly the right kidney, due to embolisation of an ulcerated plaque of the thoracic aorta

marked in the subendocardial layer and, in the case of milder stenoses, may be localised only within the subendocardial layer. Besides the detection of coronary artery disease, myocardial contrast echocardiography has been incorporated in the assessment of acute myocardial infarction and of myocardial viability. Fixed myocardial perfusion defects are those that are evident both during resting and during physical or pharmacological stress. Reversible myocardial perfusion defects (Fig. 8) are those that become evident during physical or pharmacological stress and disappear during resting [61, 62]. The same technique may be applied in the detection of damaged but viable myocardium ("hibernating myocardium") [63, 64] as dysfunctional segments demonstrating contrast enhancement have better recovery of wall motion than segments with no reflow. Myocardial contrast echocardiography offers real-time frame rates and the direct correlation between flow and wall motion. It has many potential advantages over conventional methods, particularly SPECT, with regard to both cost and exposure to ionising radiation [65], and could reduce the number of inappropriate admissions of patients with non-cardiac stress pain [66].

Contrast-enhanced ultrasound quantitation of tissue perfusion has been applied in kidneys [45, 49, 67] (Fig. 9) and renal transplants [68–70]. In patients with renal artery stenosis (Fig. 10) or other vascular abnormalities, the re-filling curve revealed an increased time-to-peak and reduced slope of the wash-in tract and maximum amplitude [49, 67–70]. Animal models were initially employed to assess the capabilities of CEUS in the detection of renal perfusion defects [71–75], which appear as single or multiple focal wedge-shaped areas of absent, diminished or delayed contrast enhancement in comparison to the adjacent renal parenchyma (Figs. 11, 12) [76, 77]. The identification of small renal perfusion defects in the sub-capsular renal region is penalised by the limited spatial resolution of CEUS which cannot identify renal perfusion defects smaller than 5 mm. Other fields of application of CEUS in tissue perfusion quantitation are the liver [78, 79], skeletal muscle [80, 81], free skin flaps [82], joints [83], testis [84, 85] and prostate [86]. Moreover, CEUS is capable of quantifying tumor tissue perfusion via their neoangiogenesis [87–94], also by the use of microbubbles targeting the tumor antigens [95].

Concluding remarks

Tissue perfusion quantitation represents one of the most promising new fields of application for CEUS. Measurement of transit time has been shown to be feasible and has started to become accepted as a clinical tool, especially in the liver. Reperfusion kinetics represents a reliable technique for obtaining semiquantitative parameters related to local tissue perfusion.

References

1. Fredriksson I, Fors C, Johansson J (2007) Laser doppler flowmetry—a theoretical framework. Department of Biomedical Engineering, Linköping University. Available via www.imt.liu.se/bit/ldf/ldfmain.html. Accessed 13 Aug 2010
2. Green MA, Mathias CJ, Willis LR et al (2007) Assessment of Cu-ETS as a PET radiopharmaceutical for evaluation of regional renal perfusion. Nucl Med Biol 34:247–255
3. Daghini E, Primak AN, Chade AR et al (2007) Assessment of renal hemodynamics and function in pigs with 64-section multidetector CT: comparison with electron beam CT. Radiology 243:405–412
4. Martin DR, Sharma P, Salman K et al (2008) Individual kidney blood flow measured with contrast-enhanced first-pass perfusion MR imaging. Radiology 246:241–248
5. Kudomi N, Slimani L, Järvisalo MJ et al (2008) Non-invasive estimation of hepatic blood perfusion from $H_2{}^{15}O$ PET images using tissue-derived arterial and portal input functions. Eur J Nucl Med Mol Imaging 35:1899–1911
6. Quaia E (2007) Microbubble ultrasound contrast agents: an update. Eur Radiol 17:1995–2008
7. Qin S, Caskey CF, Ferrara KW (2009) Ultrasound contrast microbubbles in imaging and therapy: physical principles and engineering. Phys Med Biol 54:R27–R57
8. Sboros V, Tang MX (2010) The assessment of microvascular flow and tissue perfusion using ultrasound imaging. Proc Inst Mech Eng H 224:273–290
9. Cosgrove DO, Eckersley R, Blomley M, Harvery C (2001) Quantification of blood flow. Eur Radiol 11:1338–1344
10. Cosgrove DO, Harvey C (2009) Clinical uses of microbubbles in diagnosis and treatment. Med Biol Eng Comput 47:813–826
11. Quaia E, Blomley MJK, Patel S et al (2002) Initial observations on the effect of irradiation on the liver-specific uptake of Levovist. Eur J Radiol 41:192–199
12. Yanagisawa K, Moriyasu F, Miyahara T, Yuki M, Iijima H (2007) Phagocytosis of ultrasound contrast agent microbubbles by Kupffer cells. Med Biol 33:318–325
13. Piscaglia F, Bolondi L, Italian Society for Ultrasound in Medicine and Biology (SIUMB) Study Group on Ultrasound Contrast Agents (2006) The safety of Sonovue in abdominal applications: retrospective analysis of 23188 investigations. Ultrasound Med Biol 32:1369–1375
14. Barnett SB, Duck F, Ziskin M (2007) WFUMB symposium on safety of ultrasound in medicine: conclusions and recommendations on biological effects and safety of ultrasound contrast agents, 2006. Ultrasound Med Biol 33:233–234
15. Dijkmans P, Visser C, Kamp O (2005) Adverse reactions to ultrasound contrast agents: is the risk worth the benefit? Eur J Echocardiogr 6:363–366
16. Kusnetzky L, Khalid A, Khumri T et al (2008) Acute mortality in hospitalized patients undergoing echocardiography with and without an ultrasound contrast agent: results in 18, 671 consecutive studies. J Am Coll Cardiol 51:1704–1706
17. Mulvagh SL, Vannan MA, Becher H et al (2008) American Society of Echocardiography consensus statement on the clinical applications of ultrasonic contrast agents in echocardiography. J Am Soc Echocard 21:1179–1201
18. Senior R, Becher H, Monaghan M et al (2009) Contrast echocardiography: evidence-based recommendations by European

Association of Echocardiography. Eur J Echocardiogr 10:194–212
19. Harvey CJ, Lynch M, Blomley MJ, Cosgrove DO, Eckersley RJ, Warrens AN (2001) Can renal arteriovenous transit time measured using bolus injections of the ultrasound microbubble Levovist (SHU 508A) characterize the vasculopathy in acute renal allograft rejection? (abstract) In: Radiological Society of North America scientific assembly and annual meeting program. Oak Brook, Ill: Radiological Society of North America, 2001: 418
20. Kedar RP, Cosgrove DO, McCready VR et al (1996) Microbubble contrast agent for color Doppler US: effect on breast masses. Work in progress. Radiology 198:679–686
21. Winehouse J, Douek M, Holz K et al (1999) Contrast-enhanced colour Doppler ultrasonography in suspected breast cancer recurrence. Br J Surg 86:1198–1201
22. Baz E, Madjar H, Reuss C et al (2000) The role of enhanced Doppler ultrasound in differentiation of benign vs. malignant scar lesion after breast surgery for malignancy. Ultrasound Obstet Gynecol 15:377–382
23. Blomley MJ, Albrecht T, Cosgrove DO et al (1998) Liver vascular transit time analyzed with dynamic hepatic venography with bolus injections of an US contrast agent: early experience in seven patients with metastases. Radiology 209:862–866, Erratum in: Radiology 1999: 210:882
24. Albrecht T, Blomley MJ, Cosgrove DO et al (1999) Non-invasive diagnosis of hepatic cirrhosis by transit-time analysis of an ultrasound contrast agent. Lancet 8(353):1579–1583
25. Blomley MJ, Lim AK, Harvey CJ et al (2003) Liver microbubble transit time compared with histology and Child-Pugh score in diffuse liver disease: a cross sectional study. Gut 52:1188–1193
26. Lim AK, Taylor-Robinson SD, Patel N et al (2005) Hepatic vein transit times using a microbubble agent can predict disease severity non-invasively in patients with hepatitis C. Gut 54:128–133
27. Lim AK, Patel N, Eckersley RJ et al (2006) Hepatic vein transit time of SonoVue: a comparative study with Levovist. Radiology 240:130–135
28. Hohmann J, Müller C, Oldenburg A et al (2009) Hepatic transit time analysis using contrast-enhanced ultrasound with BR1: a prospective study comparing patients with liver metastases from colorectal cancer with healthy volunteers. Ultrasound Med Biol 35:1427–1435
29. Correas JM, Burns PN, Lai X, Qi X (2000) Infusion versus bolus of an ultrasound contrast agent: in vivo dose–response measurements of BR1. Invest Radiol 35:72–79
30. Mulè S, De Cesare A, Lucidarme O, Frouin F, Herment A (2008) Regularized estimation of contrast agent attenuation to improve the imaging of microbubbles in small animal studies. Ultrasound Med Biol 34:938–948
31. Mari J, Hibbs K, Stride E, Eckersley R, Tang M (2010) An approximate nonlinear model for time gain compensation of amplitude modulated images of ultrasound contrast agent perfusion. IEEE Trans Ultrason Ferroelectr Freq Control 57:818–829
32. Phillips P, Gardner E (2004) Contrast-agent detection and quantification. Eur Radiol 14(Suppl 8):P4–P10
33. Rognin NG, Frinking P, Costa M, Arditi M (2008) In-vivo perfusion quantification by contrast ultrasound: validation of the use of linearized video data vs raw RF data. IEEE International Ultrasonics Symposium Proceedings, 1690–1693
34. Wiesmann M, Meyer K, Günter Seidel TA (2004) Parametric perfusion imaging with contrast-enhanced ultrasound in acute ischemic stroke. Stroke 35:508–513
35. Gu X, Zhong H, Wan M, Hu X, Lv D, Shen L, Zhang X (2010) Parametric perfusion imaging based on low-cost ultrasound platform. Ultrasound Med Biol 36:130–144
36. Wei K, Jayaweera AR, Firoozan S, Linka A, Skyba DM, Kaul S (1998) Quantification of myocardial blood flow with ultrasound-induced destruction of microbubbles administered as a constant venous infusion. Circulation 97:473–483
37. Potdevin TCU, Fowlkes JB, Moskalik AP, Carson PL (2004) Analysis of refill curve shape in ultrasound contrast agent studies. Med Phys 31:623–632
38. Potdevin TCU, Fowlkes JB, Moskalik AP, Carson PL (2006) Refill model of rabbit kidney vasculature. Ultrasound Med Biol 32:1331–1338
39. Metzler V, Seidel G, Wiesmann K et al (2003) Perfusion harmonic imaging of the human brain. SPIE 5035:337–348
40. Lucidarme O, Kono Y, Corbeil J, Choi SH, Mattrey RF (2003) Validation of ultrasound contrast destruction imaging for flow quantification. Ultrasound Med Biol 29:1697–1704
41. Porter TR, Xie F, Silver M, Kricsfeld D, Oleary E (2001) Real-time perfusion imaging with low mechanical index pulse inversion Doppler imaging. J Am Coll Cardiol 37:748–753
42. Arditi M, Frinking PJ, Zhou X, Rognin NG (2006) A new formalism for the quantification of tissue perfusion by the destruction replenishment method in contrast ultrasound imaging. IEEE Trans Ultrason Ferroelectr Freq Control 53:1118–1129
43. Maier P, Zierler K (1954) On the theory of indicator dilution method for the measurement of blood flow and volume. J Appl Physiol 4:308–314
44. Wei K, Ragosta M, Thorpe J, Coggins M, Moos S, Kaul S (2001) Non-invasive quantification of coronary blood flow reserve in humans using myocardial contrast echocardiography. Circulation 103:2560–2565
45. Wei K, Le E, Bin JP, Coggins M, Thorpe J, Kaul S (2001) Quantification of renal blood flow with contrast-enhanced ultrasound. J Am Coll Cardiol 37:1135–1140
46. Krix M, Kiessling F, Farhan N, Schmidt K, Hoffend J, Delorme S (2003) A multivessel model describing replenishment kinetics of ultrasound contrast agent for quantification of tissue perfusion. Ultrasound Med Biol 29:1421–1430
47. Meyer-Wiethe K, Cangür H, Seidel G (2005) Comparison of different mathematical models to analyze diminution kinetics of ultrasound contrast enhancement in a flow phantom. Ultrasound Med Biol 31:93–98
48. Lucidarme O, Franchi-Abella S, Correas JM, Bridal SL, Kurtisovski E, Berger G (2003) Blood flow quantification with contrast-enhanced US: “entrance in the section” phenomenon—phantom and rabbit study. Radiology 228:473–479
49. Quaia E, Nocentini A, Torelli L (2009) Assessment of a new mathematical model for the computation of numerical parameters related to renal cortical blood flow and fractional blood volume by contrast-enhanced ultrasound. Ultrasound Med Biol 35:616–627
50. Federlein J, Postert T, Meves S, Weber S, Przuntek H, Buttner T (2000) Ultrasonic evaluation of pathological brain perfusion in acute stroke using second harmonic imaging. J Neurol Neurosurg Psychiatry 69:616–622
51. Rim SJ, Leong-Poi H, Lindner JR et al (2001) Quantification of cerebral perfusion with real-time contrast-enhanced ultrasound. Circulation 104:2582–2587
52. Eyding J, Wilkening W, Postert T (2002) Brain perfusion and ultrasonic imaging techniques. Eur J Ultrasound 1–2:91–104
53. Holsher T, Wilkening W, Draganski B et al (2005) Transcranial ultrasound brain perfusion assessment with a contrast agent-specific imaging mode: results of a two-center trial. Stroke 36:2283–2285
54. Seidel G, Meairs S (2009) Ultrasound contrast agents in ischemic stroke. Cerebrovasc Dis 27(Suppl 2):25–39
55. Wei K, Jayaweera AR, Firoozan S et al (1998) Basis for detection of stenosis using venous administration of microbubbles during myocardial contrast echocardiography: bolus or continuous infusion? J Am Coll Cardiol 32:252–260

56. Wei K, Tong KL, Belcik T, Rafter P, Ragosta M, Wang XQ, Kaul S (2005) Detection of coronary stenoses at rest with myocardial contrast echocardiography. Circulation 112:1154–1160
57. Kaufmann BA, Wei K, Lindner JR (2007) Contrast echocardiography. Curr Probl Cardiol 32:51–96
58. Abdelmoneim SS, Mulvagh SL (2009) Stress echocardiography—state of the art. US Cardiology 6:16–26
59. Masugata H, Peters B, Lafitte S, Strachan GM, Ohmori K, De Maria AN (2001) Quantitative assessment of myocardial perfusion during graded coronary stenosis by real-time myocardial contrast refilling curves. J Am Coll Cardiol 37:262–269
60. Dijkmans PA, Senior R, Becher H et al (2006) Myocardial contrast echocardiography evolving as a clinically feasible technique for accurate, rapid, and safe assessment of myocardial perfusion: the evidence so far. J Am Coll Cardiol 48:2168–2177
61. Marwick TH, Brunken R, Meland N, Brochet E, Baer FM, Binder T et al (1998) Nycomed NC100100 Investigators. Accuracy and feasibility of contrast echocardiography for detection of perfusion defects in routine practice: comparison with wall motion and technetium-99m sestamibi single photon emission computed tomography. J Am Coll Cardiol 32:1260–1269
62. Porter TR, Xie F (2010) Myocardial perfusion imaging with contrast ultrasound. J Am Coll Cardiol Img 3:176–187
63. Shimoni S, Frangogiannis NG, Aggeli CJ et al (2003) Identification of hibernating myocardium with quantitative intravenous myocardial contrast echocardiography: comparison with dobutamine echocardiography and thallium-201 scintigraphy. Circulation 107:538–544
64. Tousek P, Penicka M, Tintera J, Linkova H, Gregor P (2008) Identification of hibernating myocardium with myocardial contrast echocardiography: comparison with late gadolinium-enhanced magnetic resonance. Int J Cardiol 128:117–120
65. Lindner JR, Kaul S (1995) Insights into the assessment of myocardial perfusion offered by different cardiac imaging modalities. J Nucl Cardiol 2:446–460
66. Gaibazzi N, Reverberi C, Squeri A et al (2009) Contrast stress echocardiography for the diagnosis of coronary artery disease in patients with chest pain but without acute coronary syndrome: incremental value of myocardial perfusion. J Am Soc Echocardiogr 22:404–410
67. Kishimoto N, Mori Y, Nishiue T et al (2003) Renal blood flow measurement with contrast-enhanced harmonic ultrasonography: evaluation of dopamine-induced changes in renal cortical perfusion in humans. Clin Nephrol 59:423–428
68. Kim JH, Eun HW, Lee HJ, Goo DE, Choi DL (2005) Clinical use of renal perfusion imaging by means of harmonic sonography with a microbubble contrast agent in patients after renal transplantation: preliminary study. J Ultrasound Med 24:755–762
69. Schwenger V, Hinkel UP, Nahm AM, Morath C, Zeier M (2006) Real-time contrast-enhanced sonography in renal transplant recipients. Clin Transplant 20:51–54
70. Kihm LP, Hinkel UP, Michael K et al (2009) Contrast-enhanced sonography shows superior microvascular renal allograft perfusion in patients switched from cyclosporine A to everolimus. Transplantation 88:261–265
71. Taylor GA, Ecklund K, Dunning PS (1996) Renal cortical perfusion in rabbits: visualization with color amplitude imaging and an experimental microbubble-based US contrast agent. Radiology 201:125–129
72. Taylor GA, Barnewolt CE, Adler BH, Dunning PS (1998) Renal cortical ischemia in rabbits revealed by contrast-enhanced power Doppler sonography. AJR Am J Roentgenol 170:417–422
73. Taylor GA, Barnewolt CE, Claudon M, Dunning P (1999) Depiction of renal perfusion defects with contrast-enhanced harmonic sonography in a porcine model. AJR Am J Roentgenol 173:757–760
74. Claudon M, Barnewolt C, Taylor GA et al (1999) Renal blood flow in pigs: changes depicted with contrast-enhanced harmonic US imaging during acute urinary obstruction. Radiology 212:725–731
75. Quaia E, Siracusano S, Palumbo A, Ciciliato S, Rossi S, Bruni S, Bussani R, Cova M (2006) Detection of focal renal perfusion defects in rabbits after sulfur hexafluoride-filled microbubble injection at low transmit power ultrasound insonation. Eur Radiol 16:166–172
76. Correas JM, Claudon M, Tranquart F, Hélenon O (2003) Contrast-enhanced ultrasonography: renal applications. J Radiol 84:2041–2054
77. Bertolotto M, Martegani A, Aiani L, Zappetti R, Cernic S, Cova MA (2008) Value of contrast-enhanced ultrasonography for detecting renal infarcts proven by contrast-enhanced CT. A feasibility study. Eur Radiol 18:376–383
78. Hancock J, Dittrich H, Jewitt DE, Monaghan GE (1999) Evaluation of myocardial, hepatic, and renal perfusion in a variety of clinical conditions using an intravenous ultrasound contrast agent (Optison) and second harmonic imaging. Heart 81:636–641
79. Gasparini C, Bertolotto M, Crocè SL, Perrone R, Quaia E, Tiribelli C (2003) Evaluation of liver parenchymal blood flow with contrast-enhanced US: preliminary results in healthy and cirrhotic patients. Acad Radiol 10:869–876
80. Lindner JR, Womack L, Barrett E, Weltman J, Price W, Harthun NL, Kaul S, Patrie JT (2008) Limb stress-rest perfusion imaging with contrast ultrasound for the assessment of peripheral arterial disease severity. J Am Coll Cardiol 1:343–350
81. Weber MA, Krix M, Jappe U et al (2005) Pathologic skeletal muscle perfusion in patients with myositis: detection with quantitative contrast-enhanced US—Initial results. Radiology 238:640–649
82. Christiansen JP, Leong-Poi H, Amiss LR, Drake DB, Kaul S, Lindner JR (2002) Skin perfusion assessed by contrast ultrasound predicts tissue survival in a free flap model. Ultrasound Med Biol 28:315–320
83. Klauser A, Demharter J, De Marchi A et al (2005) Contrast enhanced gray-scale sonography in assessment of joint vascularity in rheumatoid arthritis: results from the IACUS study group. Eur Radiol 15:2404–2410
84. Paltiel HJ, Kalish LA, Susaeta RA, Frausher F, O'Kane PL, Freitas-Filho LG (2006) Pulse Inversion US imaging of testicular ischemia: quantitative and qualitative analyses in a rabbit model. Radiology 239:718–729
85. Chen L, Zhan WW, Shen ZJ et al (2009) Blood perfusion of the contralateral testis evaluated with contrast-enhanced ultrasound in rabbits with unilateral testicular torsion. Asian J Androl 11:253–260
86. Eckersley RJ, Sedelaar JP, Blomley MJK et al (2002) Quantitative microbubble enhanced transrectal ultrasound as a tool for monitoring hormonal treatment of prostate carcinoma. Prostate 51:256–267
87. Krix M, Kiessling F, Vosseler S et al (2003) Sensitive noninvasive monitoring of tumor perfusion during antiangiogenic therapy by intermittent bolus-contrast power Doppler sonography. Cancer Res 63:8264–8270
88. Lassau N, Chami L, Benatsou B, Peronneau P, Roche A (2007) Dynamic contrast-enhanced ultrasonography (DCE-US) with quantification of tumor perfusion: a new diagnostic tool to evaluate the early effects of antiangiogenic treatment. Eur Radiol 17(Suppl 6):F89–F98
89. Lassau N, Lamuraglia M, Chami L et al (2006) Gastrointestinal stromal tumors treated with imatinib: monitoring response with contrast-enhanced sonography. AJR Am J Roentgenol 187:1267–1273

90. Yankeelov TE, Niermann KJ, Huamani J et al (2006) Correlation between estimates of tumor perfusion from microbubble contrast-enhanced sonography and dynamic contrast-enhanced magnetic resonance imaging. J Ultrasound Med 25:487–497
91. Niermann KJ, Fleischer AC, Huamani J et al (2007) Measuring tumor perfusion in control and treated murine tumors: correlation of microbubble contrast-enhanced sonography to dynamic contrast-enhanced magnetic resonance imaging and fluorodeoxyglucose positron emission tomography. J Ultrasound Med 26:749–756
92. McCarville MB, Streck CJ, Dickson PV, Li CS, Nathwani AC, Davidoff AM (2006) Angiogenesis inhibitors in a murine neuroblastoma model: quantitative assessment of intratumoral blood flow with contrast-enhanced gray-scale US. Radiology 240:73–81
93. Stieger SM, Bloch SH, Foreman O, Wisner ER, Ferrara KW, Dayton PA (2006) Ultrasound assessment of angiogenesis in a matrigel model in rats. Ultrasound Med Biol 32:673–681
94. Guibal A, Taillade L, Mulè S et al (2010) Noninvasive contrast-enhanced US quantitative assessment of tumor microcirculation in a murine model: effect of discontinuing anti-VEGF therapy. Radiology 254:420–429
95. Ellegala DB, Leong-Poi H, Carpenter JE et al (2003) Imaging tumor angiogenesis with contrast ultrasound and microbubbles targeted to $\alpha_v\beta_3$. Circulation 108:336–341